Supplemental Material

Tuning the ground state of cuprate high-critical-temperature superconducting thin films by nanofaceted substrates

G. Mirarchi, S. Caprara, C. Di Castro, M. Grilli

Dipartimento di Fisica, Università di Roma "La Sapienza", P.^{le} Aldo Moro 5, 00185 Roma, Italy

R. Arpaia, E. Wahlberg, A. Kalaboukhov, T. Bauch, F. Lombardi

Quantum Device Physics Laboratory, Department of Microtechnology and Nanoscience, Chalmers University of Technology, SE-41296 Göteborg, Sweden

G. Seibold

Institut für Physik, BTU Cottbus-Senftenberg, D-03013 Cottbus, Germany

I. OVERVIEW

The theoretical considerations in the main paper start from a tight-binding model which captures the coupling of states from the CuO_2 layer with those of the nano-facets (or steps) on the substrate. In Sec. II we detail how within this model a nematic electronic structure can be obtained, based on the coherent potential approximation (CPA). The resulting nematic Fermi surface can be well described by an anisotropic tight-binding model [see Fig. 2(c) of the main paper] which is the basis for the investigation of CDW formation within the frustrated phase separation scenario in a nematic system. The details of the corresponding calculation are given in Sec. III.

II. CPA CALCULATION OF THE FERMI SURFACE

Our effective model reads

$$H = \sum_{ij,\sigma} t_{ij} c^\dagger_{i,\sigma} c_{j,\sigma} + t_\perp \sum_{n,\sigma} \sum_{m=1}^{L} \left[c^\dagger_{\mathbf{R}_n+m\mathbf{b},\sigma} d_{\mathbf{R}_n+m\mathbf{b},\sigma} + h.c. \right] + V_{sub} \sum_{n,\sigma} \sum_{m=1}^{L} d^\dagger_{\mathbf{R}_n+m\mathbf{b},\sigma} d_{\mathbf{R}_n+m\mathbf{b},\sigma} \tag{S1}$$

where $c^{(\dagger)}_{i,\sigma}$ and $d^{(\dagger)}_{i,\sigma}$ denote annihilation (creation) operators for the electronic states in the CuO_2 layers and undercoordinated facet (or step) states on the substrate, respectively. R_n denotes the starting sites of the latter 1-D structures with length L and local potentials $-V_{sub}$ (see Fig. S1). The hopping term $t_{i,j}$ will be considered below only at the level of nearest ($\sim t$) and next-nearest neighbor ($\sim t'$) .

In a first step we eliminate the hopping $t_\perp$ between layer and undercoordinated substrate states by diagonalizing the corresponding local coupling hamiltonian

$$H^{coup}_{n,m,\sigma} = \begin{pmatrix} c^\dagger_{i,\sigma} \\ d^\dagger_{i,\sigma} \end{pmatrix} \begin{pmatrix} 0 & t_\perp \\ t_\perp & -V_{sub} \end{pmatrix} \begin{pmatrix} c_{i,\sigma} \\ d_{i,\sigma} \end{pmatrix} \tag{S2}$$

so that the coupled layer states are renormalized by an effective local chemical potential

$$V_{eff} = \frac{1}{2} \left[\sqrt{V^2_{sub} + 4t^2_\perp} - V_{sub} \right] . \tag{S3}$$

As a result we obtain an effective hamiltonian for the coupled layer system [Eq. (1) in the main paper] which reads

$$H = \sum_{ij,\sigma} t_{ij} c^\dagger_{i,\sigma} c_{j,\sigma} + V_{eff} \sum_{n,\sigma} \sum_{m=1}^{L} c^\dagger_{\mathbf{R}_n+m\mathbf{b},\sigma} c_{\mathbf{R}_n+m\mathbf{b},\sigma} \, . \tag{S4}$$

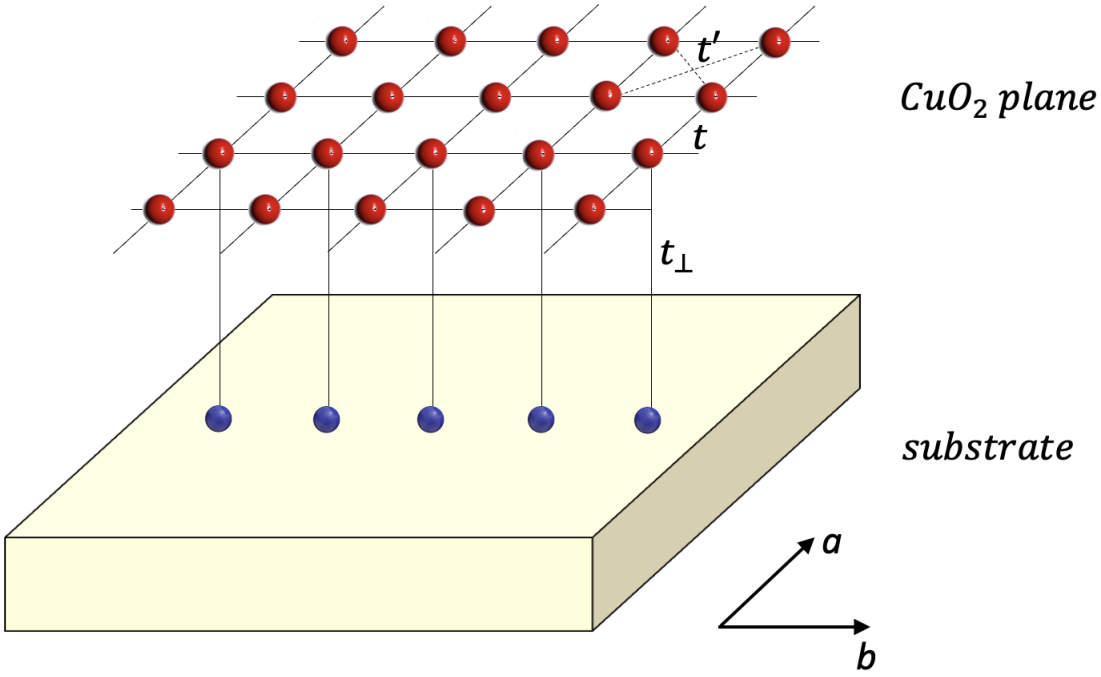

FIG. S1. Schematic view of the planar tight-binding model with the CuO_2 layer (atoms, red dots) effectively coupled by the perpendicular hopping $t_\perp$ to the substrate facets or steps (blue dots).

Moreover, due to the very anisotropic shape of the nanofacets (or steps) we can take the limit $L \to \infty$ so that our model corresponds to charge carriers in the CuO_2 layer which are subject to infinitely extended one-dimensional potentials along the b-direction and randomly distributed with an area fraction of nanofacets (steps) given by the parameter *'f'*.

The resulting electronic structure can be most conveniently obtained from the coherent-potential approximation (CPA) [1] with a self-energy

$$\Sigma(k_b,\omega) = \frac{fV_0}{1-(V_0-\Sigma(k_b,\omega))\bar{G}(k_b,\omega-\Sigma(k_b,\omega))} \tag{S5}$$

with

$$\bar{G}(k_b,\omega) = \frac{1}{N}\sum_{k_a}\frac{1}{\omega+2t\cos(k_b)+\gamma(k_b)\cos(k_a)} \tag{S6}$$

$$= \frac{1}{\sqrt{[\omega+2t\cos(k_b)]^2-\gamma^2(k_b)}} \tag{S7}$$

$$\gamma(k_b) = -2t-4t'\cos(k_b)\,. \tag{S8}$$

Fig. S2 shows the real- and imaginary part of the resulting self-energy which both display a dispersing behavior with $\omega \sim \cos(k_b)$ and $\Sigma' > 0$. At the Fermi energy (dashed line in

Fig. S2a) the real part is essentially zero at $k_b = 0$ but gradually increases towards larger momenta where it thus adds an additional contribution to the hopping along k_b. As a consequence the kinetic energy along the k_b-direction becomes enhanced and results in a nematic Fermi surface which is shown in Fig. 3 of the main paper. The enhancement of the imaginary part of the self-energy for small k_b at the Fermi energy is then responsible for the blurred feature around the $(\pm\pi, 0)$ regions in Fig. 3(c).

This Fermi surface can also be modeled [see Fig. 2(c) of the main paper] within an effective one-band model where the nearest-neighbor hopping is enlarged (reduced) along the orthorhombic b- (a-) direction i.e.

$$\begin{aligned} \varepsilon_k^0 &= -2t(1+\alpha)\cos(k_b) - 2t(1-\alpha)\cos(k_a) \\ &- 4t'\cos(k_b)\cos(k_a) \end{aligned} \tag{S9}$$

with α denoting the anisotropy parameter.

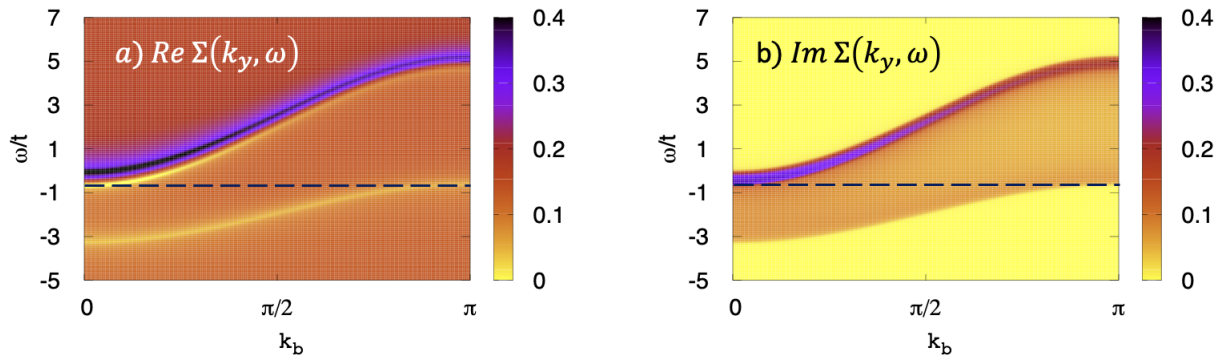

FIG. S2. Real- (a) and imaginary (b) part of the CPA self-energy for a disordered array of 'defect lines' ($f = 0.15$) as a function of ω and k_y. The horizontal dashed line indicates the location of the Fermi energy. Here $t'/t = -0.17$ and $V_{eff} = 1$, while the doping is $p = 0.15$,.

III. TIME-DEPENDENT SLAVE-BOSON THEORY

Our model is based on the slave-boson approach for the $U \to \infty$ Hubbard model [2] where the Hilbert space is enlarged by auxiliary bosons $b_i^{(\dagger)}$. The resulting hamiltonian reads

$$H = \sum_{ij\sigma} t_{ij} b_i b_j^\dagger f_{i\sigma}^\dagger f_{j\sigma} \tag{S10}$$

where in addition at each site the constraint

$$\sum_{\sigma} f_{i\sigma}^{\dagger} f_{i\sigma} + b_i^{\dagger} b_i = 1 \tag{S11}$$

has to be fulfilled. This constraint guarantees that the site occupation of the quasiparticles $\sum_{\sigma} n_{i,\sigma} \leq 1$ and simultaneously restricts the Hilbert space to the correct physical sector.

The mean-field energy functional reads

$$E_0 = \sum_{ij\sigma} \sqrt{1-\langle n_i \rangle}\sqrt{1-\langle n_j \rangle}\langle f_{i\sigma}^{\dagger} f_{j\sigma}\rangle \tag{S12}$$

where we have set $b_i \to \langle b_i \rangle = \sqrt{1-\langle n_i \rangle}$ with $\langle n_i \rangle = \sum_{\sigma}\langle f_{i\sigma}^{\dagger} f_{i\sigma}\rangle$.

We now expand the functional Eq. (S12) up to second order in the density fluctuations

$$\begin{aligned}
\sqrt{1-\langle n_i \rangle} &\approx \sqrt{1-\langle n \rangle} - \frac{1}{2\sqrt{1-\langle n \rangle}}\delta\langle n_i \rangle \\
&- \frac{1}{8}\frac{1}{(1-\langle n \rangle)^{3/2}}(\delta\langle n_i \rangle)^2 \\
\langle f_{i\sigma}^{\dagger} f_{j\sigma}\rangle &= \langle f_{i\sigma}^{\dagger} f_{j\sigma}\rangle_0 + \delta\langle f_{i\sigma}^{\dagger} f_{j\sigma}\rangle
\end{aligned}$$

where $\langle n \rangle \equiv \langle n_i \rangle_0$ is the saddle-point value for the charge density for the homogeneous system.

The second order contribution reads

$$\begin{aligned}
\delta^{(2)}E &= \sum_{ij\sigma} t_{ij}\left[\langle f_{i\sigma}^{\dagger} f_{j\sigma}\rangle_0 \left(\frac{1}{4(1-\langle n \rangle)}\delta\langle n_i \rangle\delta\langle n_j \rangle\right.\right. \\
&- \frac{1}{8}\frac{1}{1-\langle n \rangle}\left[(\delta\langle n_i \rangle)^2 + (\delta\langle n_j \rangle)^2\right]\Big) \\
&- \left.\frac{1}{2}(\delta\langle n_i \rangle + \delta\langle n_j \rangle)\delta\langle f_{i\sigma}^{\dagger} f_{j\sigma}\rangle\right] .
\end{aligned}$$

We now define the Fourier transformed fluctuations

$$\begin{aligned}
\delta\rho_q &= \sum_{k\sigma} \delta\langle f_{k+q,\sigma}^{\dagger} f_{k,\sigma}\rangle \\
\delta T_q &= \frac{1}{2}\sum_{k\sigma}(\varepsilon_{k+q}^0 + \varepsilon_k^0)\delta\langle f_{k+q,\sigma}^{\dagger} f_{k,\sigma}\rangle
\end{aligned}$$

so that the second order expansion can be written as

$$\delta^{(2)}E = \frac{1}{2N}\sum_q \begin{pmatrix} \delta\rho_q \\ \delta T_q \end{pmatrix} \underbrace{\begin{pmatrix} V_{\rm res}(q) & -1 \\ -1 & 0 \end{pmatrix}}_{\equiv M_q} \begin{pmatrix} \delta\rho_{-q} \\ \delta T_{-q} \end{pmatrix} \tag{S13}$$

with

$$V_{\rm res}(q) = \frac{1}{2\,(1-\langle n\rangle)}\left[-e_0 + \frac{1}{N}\sum_{k\sigma}\varepsilon^0_{k+q} n_{k\sigma}\right] \tag{S14}$$

and e_0 is the unrenormalized ground state energy. Upon including long-range Coulomb and electron-phonon interaction, $V^{coul}(q)$ and $V^{ph}(q)$, the residual repulsion $V_{\rm res}(q)$ in Eq. (S13) should be replaced by

$$V_{tot}(q) = V_{\rm res}(q) + V^{ph}(q) + V^{coul}(q)\,. \tag{S15}$$

The present approach differs from that in Ref. 3 which uses the radial gauge and therefore considers fluctuations in the boson amplitude and the Lagrange multiplier λ_i. Here we have fluctuations in the local and transitive densities which, however, lead to the same results for the correlations of physical quantities.

By defining the susceptibility matrix

$$\underline{\underline{\chi_q}} = \begin{pmatrix} \chi_q^{\rho\rho} & \chi_q^{\rho T} \\ \chi_q^{T\rho} & \chi_q^{TT} \end{pmatrix} = \begin{pmatrix} \langle \rho_q \rho_{-q}\rangle & \langle \rho_q T_{-q}\rangle \\ \langle T_q \rho_{-q}\rangle & \langle T_q T_{-q}\rangle \end{pmatrix}$$

one can perform a RPA resummation

$$\underline{\underline{\chi_q}} = \underline{\underline{\chi^0_q}} + \underline{\underline{\chi^0_q}}\,\underline{\underline{M_q \chi_q}}$$

and the non-interacting susceptibities can be evaluated from

$$\underline{\underline{\chi^0_q}} = \frac{1}{N}\sum_{k\sigma}\begin{pmatrix} 1 & \frac{1}{2}(\varepsilon^0_k + \varepsilon^0_{k+q}) \\ \frac{1}{2}(\varepsilon^0_k + \varepsilon^0_{k+q}) & \frac{1}{4}(\varepsilon^0_k + \varepsilon^0_{k+q})^2 \end{pmatrix} \frac{n_{k+q,\sigma} - n_{k,\sigma}}{\varepsilon_{k+q} - \varepsilon_k}\,.$$

Here $\varepsilon_k \equiv (1-\langle n\rangle)\varepsilon^0_k$ is the renormalized dispersion.

In particular the dressed susceptibility for the local fluctuations is given by

$$\chi_q^{\rho\rho} = \frac{\chi_q^{\rho\rho,0}}{Det|1 - M_q\chi_q|}$$

from which one can define an effective interaction according to

$$\chi_q^{\rho\rho} \equiv \frac{\chi_q^{\rho\rho,0}}{1 - V_q^{eff}\chi_q^{\rho\rho,0}}$$

with

$$V_{\rm eff}(q) = \frac{1 - Det|1 - M_q\chi_q|}{\chi_0^{\rho\rho}}\,. \tag{S16}$$

For not too large momenta this effective interaction differs from V_q just by a constant offset, i.e. $V_{\rm eff}(q) \approx V_q + V_0$.

IV. ANISOTROPY OF THE INTERACTIONS ENTERING THE FRUSTRATED PHASE SEPARATION SCENARIO

A. Anisotropy of the residual repulsion

For the dispersion Eq. (S9) and small momenta the residual repulsion Eq. (S14) takes the form

$$V_{\rm res}(q) \;=\; \frac{1}{2\delta}\left[(1+\alpha)t_x q_x^2 + (1-\alpha)t_y q_y^2 + t_{xy}(q_x^2+q_y^2)\right] \tag{S17}$$

with $t_{x/y} = t/N\sum_{k\sigma}\cos(k_{x/y})n_{k\sigma}$ and $t_{xy} = 2t'/N\sum_{k\sigma}\cos(k_x)\cos(k_y)n_{k\sigma}$. Since for small (positive) α, $t_{x/y}$ increases / decreases with α the residual repulsion is larger in the direction of enhanced kinetic energy, i.e. along the b-direction.

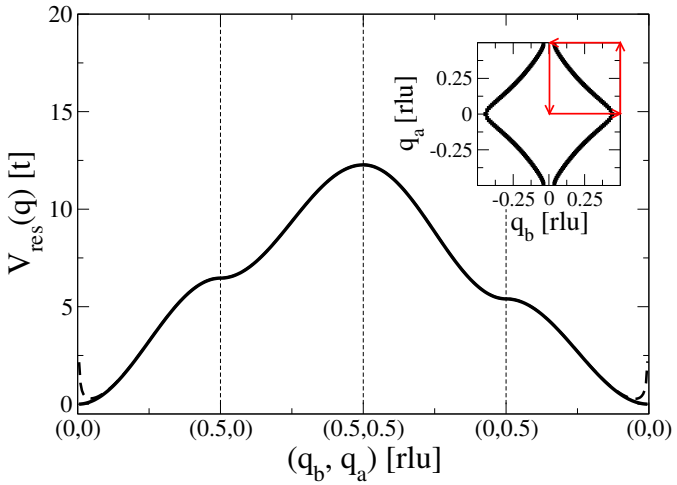

FIG. S3. Residual repulsion $V_{\rm res}$ (solid line) along the momentum cut shown in the inset which also displays the Fermi surface for the considered parameters: $\delta = 0.13$, $t'/t = -0.15$, $\alpha = 0.015$. The dashed line includes the long range Coulomb interaction, cf. Sec. IV B.

Fig. S3 shows $V_{\rm res}$ from Eq. (S14) along the momentum cut $(0,0) \to (0.5,0) \to (0.5,0.5) \to (0,0.5) \to (0,0)$. Clearly, the anisotropy in the electronic structure $\alpha = 0.015$ (cf. inset for the corresponding Fermi surface) leads to an enhanced repulsion along the b-direction.

B. Anisotropy of the long-range Coulomb interaction

Analogous to the approach in Ref. 3 we can evaluate the long-range Coulomb interaction for a single orthorhombic layer (lattice constants a,b) embedded into a 3D system with layer stacking and distance d between layers. The result for this Coulombic interaction is

$$H^{coul} = \frac{V_{coul}}{2N} \sum_q \frac{1}{A^2(q) - 1} \delta\rho_q \delta\rho_{-q} \tag{S18}$$

with

$$A_q = \frac{\varepsilon_\parallel}{\varepsilon_\perp} \frac{d^2}{a^2} \left[\cos(aq_x) - 1 + \frac{a^2}{b^2} (\cos(bq_y) - 1) \right] - 1 \,.$$

Taking the same values as in Ref. 3 $\varepsilon_\parallel \approx 30$, $\varepsilon_\perp \approx 5$, $d/a \approx 3$ yields $\frac{\varepsilon_\parallel}{\varepsilon_\perp} \frac{d^2}{a^2} = 54$. For the strained films of YBCO grown on MgO one finds [7] $a/b = 3.82/3.89 \approx 0.98$.

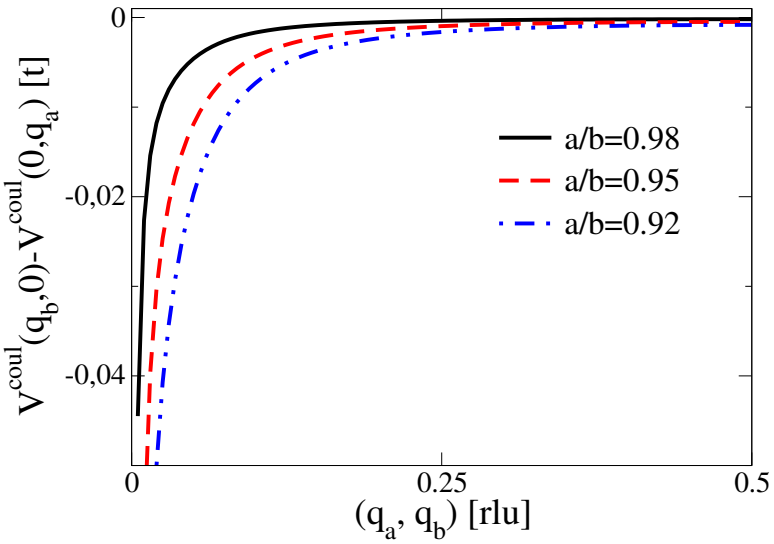

FIG. S4. Difference between Coulomb interactions along b- and a-direction for different orthorhombicities a/b. $V_{coul}/t = 0.5$.

Fig. S4 shows the difference between the Coulomb interaction along the b-axis and the a-axis. Obviously the orthorhombicity makes the system more repulsive along a, in particular at small transferred momenta. However, as compared to the residual repulsion $V_{\rm res}$, the long-range Coulomb interaction has only a minor influence on the anisotropy of the CDW.

C. Anisotropy of the bare charge susceptibility

Fig. S5 shows the momentum dependence of the static bare local charge susceptibility $\chi^0_{\rho\rho}(q, \omega = 0)$ as obtained from the dispersion Eq. (S9). Four peaks are visible in the local charge correlations which are associated with the scattering vectors indicated in the inset to Fig. S5. The two nesting vectors (red) which connect the tips at $(0.5, 0)$ and $(0, 0.5)$, respectively, are visible as peaks in $\chi^0_{\rho\rho}(q)$ along the b-direction $(q_b, 0)$ (indicated by the red dashed circle) whereas the scan along the a-direction $(0, q_a)$ is featureless with a concomitant reduction of the (local) charge correlations. The larger charge correlations around $(0.5, 0.5)$ (blue dashed circle) are due to the scattering from one tip at $(0.5, 0)$ to the other at $(0, 0.5)$ (blue arrows in the inset). However, as we discuss in the main paper this latter scattering will be suppressed due to the residual repulsion which is also large for large momentum transfers, cf. Fig. S3, so that only the scattering along the b-direction survives. Therefore an appropriate treatment of strong correlations is inevitable in order to properly account for the experimentally observed orientation of CDW in cuprates along the Cu-O bond direction.

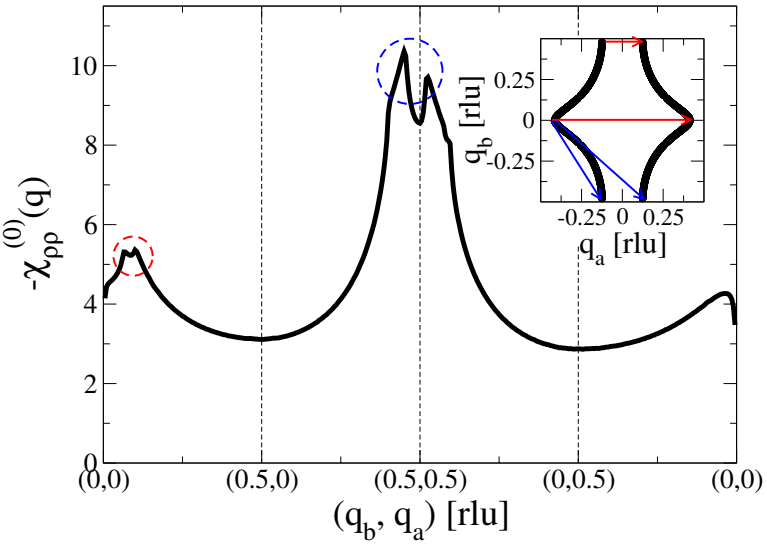

FIG. S5. Local charge correlations for $\omega = 0$ along the momentum cut indicated in the inset to Fig. S3. The arrows in the inset report the dominant scattering vectors along the horizontal (red) and diagonal (blue) directions (for clarity the Fermi surface has been drawn for a larger anisotropy). Parameters: $n = 0.87$, $t'/t = -0.15$, $\alpha = 0.015$.

[1] B. Velický, S. Kirkpatrick, and H. Ehrenreich Phys. Rev. **175**, 747 (1968).

[2] S. E. Barnes, J. Phys. F **6**, 1375 (1976); P. Coleman, Phys. Rev. B **29**, 3035 (1984); N. Read and D. M. Newns, J. Phys. C **16**, 3273 (1983).

[3] F. Becca, M. Tarquini, M. Grilli, and C. Di Castro, Phys. Rev. B **54**, 12443 (1996).

[4] C. Castellani, C. Di Castro, and M. Grilli, Phys. Rev. Lett. **75**, 4650 (1995).

[5] T. Cuk, D. H. Li, X. J. Zhou, Z.-X. Shen, T. P. Devereaux, and N. Nagaosa, Phys. Stat. Sol. (b) **242**, 11 (2005).

[6] O. Gunnarsson and O. Rösch, J. Phys.: Condens. Matter **20**, 043201 (2008).

[7] E. Wahlberg, R. Arpaia, G. Seibold, M. Rossi, R. Fumagalli, E. Trabaldo, N. B. Brookes, L. Braicovich, S. Caprara, U. Gran, G. Ghiringhelli, T. Bauch, e F. Lombardi, Science **373**, 1506 (2021) .